MICROSTRUCTURAL CHARACTERIZATION OF TiO2–II IN THE CHICXULUB PEAK RING.

Martin Schmieder[1,2], Timmons M. Erickson[3], David A. Kring[1,2] and the IODP–ICDP Expedition 364 Science Party, [1]Lunar and Planetary Institute – USRA, Houston, TX 77058 USA (schmieder@lpi.usra.edu), [2]NASA–SSERVI, [3]Jacobs–JETS, NASA–JSC, Houston, TX 77058 USA.

Introduction: The peak ring of the ~180 km-diameter Chicxulub impact crater on the Yucatán Peninsula, Mexico, was recently drilled during IODP–ICDP Expedition 364, producing core M0077A [1]. The new core provides insights into the anatomy, composition, tectonic deformation, shock metamorphism, and post-impact overprint of crater-filling impactites and crystalline basement rocks [2]. The basement rocks were shocked to ~12.5–17.5 GPa [3], uplifted, and hydrothermally altered [4]. This study presents a combined Raman spectroscopic and electron backscatter diffraction (EBSD) study of TiO2–II, a high-pressure polymorph of TiO2 with an α-PbO2 structure (orthorhombic; space group *Pbcn*; density 4.34 g/cm^3 [5,6]), in shocked granitoid rock of the Chicxulub peak ring.

Sample and Analytical Methods: We selected shocked granitoid sample 174-2 (core depth 949 m below seafloor [1,2,7]) from the Chicxulub peak ring for high-resolution analyses. The granitoid rock contains mm-sized aggregates of TiO2 crystals replacing altered euhedral titanite. The sample was analyzed using a Leica DMLP optical microscope; a 7600f JEOL field emission gun scanning electron microscope (FEG-SEM); a CAMECA SX 100 electron microprobe; a Jobin–Yvon Horiba LabRAM HR 800 μ-Raman spectrometer (514 nm Ar laser; ~1 μm spot diameter); and an Oxford Instruments Symmetry EBSD detector on the JEOL FEG-SEM (20 kV, 16 nA, 100 nm step size for phase and orientation mapping).

Results: Individual TiO2 crystals in sample 174-2 are up to ~70 μm in length and appear brown-translucent under the optical microscope. The TiO2 grains commonly occur as euhedral to subhedral crystals. Micro-Raman analysis of TiO2 crystals produced spectra with distinct bands at *ca*. 149, 173, 287, 315, 340, 356, and 532 wavenumbers (cm^{-1}) [7], in close agreement with Raman spectra for the high-pressure polymorph TiO2–II [5,8] (Fig. 1). Some spectra reveal additional bands at 442 and 610 cm^{-1}, indicating the presence of rutile. No Raman peaks typical of anatase or brookite were obtained in sample 174-2. Backscattered-electron (BSE) imaging reveals lamellar and locally granular microtextures, as well as subparallel and intersecting sets of fractures within individual TiO2 crystals (Fig. 2). Electron microprobe results show the

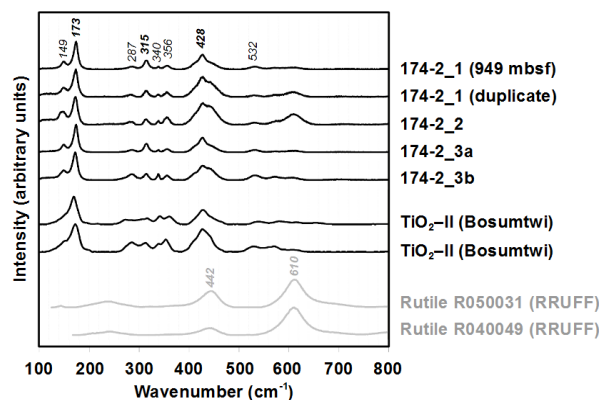TiO2 crystals contain ≤2.5 wt% Fe2O3, ≤1.5 wt% Nb2O5, ≤0.4 wt% SiO2, and ≤0.3 wt% Ta2O5.

Fig. 1: Raman spectra for TiO2–II in granitoid rock of the Chicxulub peak ring (sample 174-2), TiO2–II from the Bosumtwi impact crater, Ghana [8], and reference spectra for rutile (RRUFF database [20]). Reference spectra for anatase and brookite are not shown. The position of laser spots in the Chicxulub sample is indicated in Fig. 2.

High-resolution EBSD mapping of individual TiO2 crystals (Fig. 2), calibrated for rutile, anatase, brookite, and TiO2–II (i.e., orthorhombic TiO2 of Laue group *mmm* [9]), show a complex arrangement of locally cross-cutting lamellar and granular subdomains within each crystal investigated. EBSD phase maps reveal that the grains are composed of different TiO2 polymorphs: (1) TiO2–II, which forms larger, coherent, and commonly elongated lamellar domains that make up ~30 to 90% of the crystals; (2) rutile, in the form of microcrystalline granules and lamellae that locally occur between coarser-crystalline TiO2–II; and (3) minor anatase not detected in Raman spectra, found along the margins of the TiO2 crystals and within the surrounding matrix. The TiO2–II correlates with slightly brighter domains in high-contrast BSE images (Fig. 2). Internal cross-cutting relationships suggest the microcrystalline-granular rutile overprints shock-produced TiO2–II. EBSD orientation maps and pole figures show that individual TiO2–II lamellae are related to one another by rational twin orientations, which likely formed by transformation twinning. Interphase misorientations between shock-produced TiO2–II and neocrystalline rutile granules are systematically aligned, indicating that the solid-state reversion to rutile is crystallographically controlled.
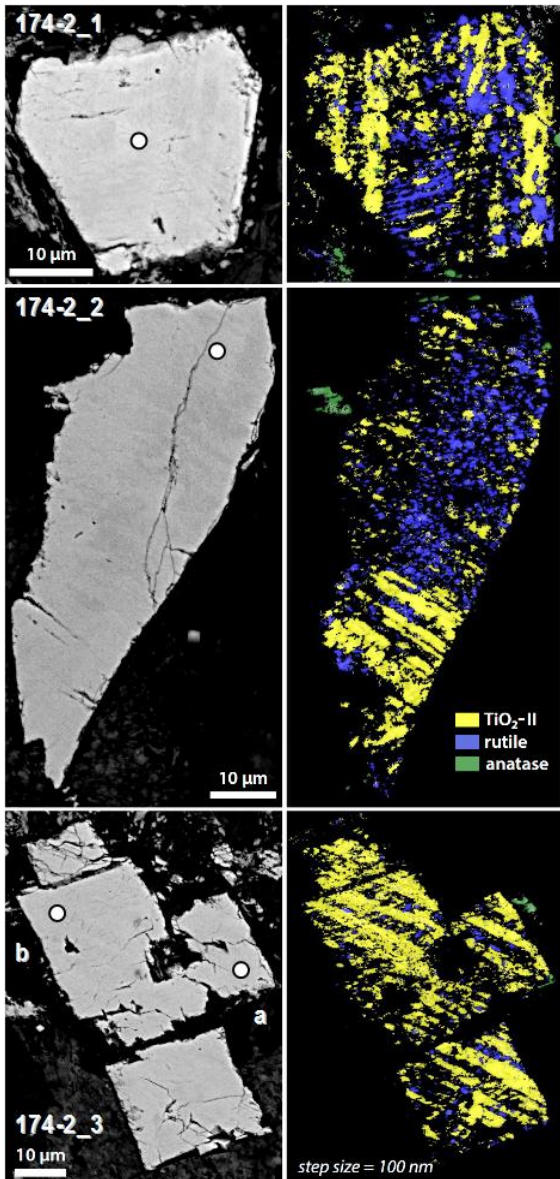
Fig. 2: Backscattered electron images (left) and corresponding EBSD phase maps (right) of TiO_2 crystals in Chicxulub peak-ring sample 174-2. White spots and labels indicate positions where Raman spectra (see Fig. 1) were collected.

Discussion and Conclusions: The discovery of TiO_2–II in rocks from the Chicxulub crater is the latest addition to a short list of terrestrial impact structures and distal ejecta layers where this shock-produced high-pressure polymorph is found [5,8,10-13]. Notably, peak-ring sample 174-2 hosts an outstanding natural occurrence of TiO_2–II, both in terms of crystal abundance and the size of individual crystals. The TiO_2–II in this and other Expedition 364 core samples [1,2] is the product of a long and complex pre-, syn-, and post-impact history recorded in Chicxulub's peak-ring lithologies. Based on our petrologic and micro-structural observations of TiO_2 grains, we propose the

following sequence of geologic events: (1) Around 340 Ma, granitoid plutons crystallized in the Maya Block [14], as indicated by U–Pb ages for magmatic titanite [7]. (2) Between ~340 Ma and 66 Ma, titanite in the granitoid rock was altered to rutile and/or anatase (+calcite, +quartz), likely during a pre-impact regional magmatic and/or hydrothermal event, and pre-sumably under high CO_2 activity [15]. (3) During the 66 Ma Chicxulub impact, rutile and/or anatase partially to fully transformed to the high-pressure polymorph TiO_2–II at shock pressures ~12.5–17.5 GPa [3] (consistent with experimental transformation pressure constraints of ~13–20 GPa [16,17]). The shock-induced transformation to TiO_2–II may have been facil-itated by pre-impact heating of the peak ring lithologies at ~8–10 km depth [1] to ~200–250 °C (at a typical geothermal gradient of ~25 °C/km); shock metamor-phic overprint of the granitoid rock contributed some additional ~100–150 °C [18]. Finally, (4) the newly formed Chicxulub crater, including shocked and uplift-ed rocks in its peak ring, hosted a long-lived post-impact hydrothermal system [4,19]. As the peak ring cooled, TiO_2–II incompletely back-transformed to neoblastic granules of rutile (Fig. 2).

TiO_2–II is stable below 340°C, but rapidly (within minutes to weeks) reverts to rutile at >440–500°C [13,16]. The formation and preservation of TiO_2–II in the Chicxulub peak ring, thus, places new petrologic constraints on shock conditions and post-impact tem-peratures inside the peak ring during crater cooling. Chicxulub's peak-ring lithologies must have cooled below 340°C relatively quickly (or did not significantly exceed those temperatures in the first place), so as to preserve much of the shock-produced TiO_2–II. Furthermore, these results suggest that TiO_2–II may be a common shock indicator at terrestrial impact struc-tures, including those that experienced vigorous and long-lived post-impact hydrothermal alteration.

References: [1] Morgan J. V. et al. (2016) *Science, 354*, 878–882. [2] Gulick S. P. S. et al. (2017) Exp. 364 Prelim. Rep., IODP, 38 pp. [3] Rae A. S. P. et al. (2017) *LPS XLVIII*, abstr. #1934. [4] Kring D. A. et al. (2017) *LPS XLVIII*, abstr. #1212. [5] El Goresy A. et al. (2001) *EPSL*, *192*, 485–495. [6] Shen P. et al. (2001) *Int. Geol. Rev.*, *43*, 366–378. [7] Schmieder M. et al. (2017) 80th MetSoc, abstr. #6134. [8] McHone F. et al. (2008) *LPS XXXIX*, abstr. #2450. [9] Grey I. et al. (1988) *Mat. Sci. Bull., 23*, 743–753. [10] Chen M. et al. (2013) *Chinese Sci. Bull.*, *58*, 4655–4662. [11] Jackson, J. C. et al. (2006) *Am. Mineral.*, *91,* 604–608. [12] Glass B. P. and Fries M. (2008) *MAPS*, *43*, 1487–1496. [13] Smith F. C. et al. (2016) *Geology*, *44*, 775–778. [14] Kring D.A. (2005) *Chem. d. Erde*, *65*, 1–46. [15] Broska I. et al. (2007) *Lithos*, *95*, 58–71. [16] Linde R. K. and DeCarli P. S. (1969) *J. Chem. Phys.*, *50*, 319–325. [17] Syono Y. et al. (1987) in *High-Pressure Re-search in Mineral Physics*, pp. 385–392. [18] Stöffler D. (1984) *J. Non-Cryst. Solids*, *67,* 465–502. [19] Abramov O. and Kring D. A. (2007) *MAPS*, *42*, 93–112. [20] http://rruff.info, online.